Original Paper

Cells Tissues Organs

Cells Tissues Organs 2014;200:349–362
DOI: 10.1159/000435875

Accepted after revision: June 10, 2015
Published online: August 14, 2015

Multiscale Characterization of Impact of Infarct Size on Myocardial Remodeling in an Ovine Infarct Model

Pei Zhang Tielou Li Bartley P. Griffith Zhongjun J. Wu

Artificial Organs Laboratory, Department of Surgery, University of Maryland School of Medicine, Baltimore, Md., USA

Key Words
Animal model · Cardiac remodeling · Multiscale characterization · Myocardial infarction

Abstract
The surviving myocardium initially compensates the loss of injured myocardium after myocardial infarction (MI) and gradually becomes progressively dysfunctional. There have been limited studies on the effect of infarct size on temporal and spatial alterations in the myocardium during progressive myocardial remodeling. MI with three infarct sizes, i.e. 15, 25 and 35% of the left ventricular (LV) wall, was created in an ovine infarction model. The progressive LV remodeling over a 12-week period was studied. Echocardiography, sonomicrometry, and histological and molecular analyses were carried out to evaluate cardiac function, regional tissue contractile function, structural remodeling and cardiomyocyte hypertrophy, and calcium handling proteins. Twelve weeks after MI, the 15, 25 and 35% MI groups had normalized LV end diastole volumes of 1.4 ± 0.2, 1.7 ± 0.3 and 2.0 ± 0.4 ml/kg, normalized end systole volumes of 1.0 ± 0.1, 1.0 ± 0.2 and 1.3 ± 0.3 ml/kg and LV ejection fractions of 43 ± 3, 42 ± 6 and 34 ± 4%, respectively. They all differed from the sham group ($p < 0.05$). All the three MI groups exhibited larger wall areal expansion (remodeling strain), larger cardiomyocyte size and altered expression of calcium handing proteins in the adjacent myocardium compared to the remote counterpart from the infarct. A significant correlation was found between cardiomyocyte size and remodeling strain in the adjacent zone. A comparative analysis among the three MI groups showed that a larger infarct size (35 vs. 15% MI) was associated with larger remodeling strain, more serious impairment in the cellular structure and composition, and regional contractile function at regional tissue level and LV function at organ level.

Abbreviations used in this paper

ED	end diastole
ES	end systole
HE	hematoxylin-eosin
LV	left ventricular or left ventricle
LVEDV	left ventricular end-diastolic volume
LVEF	left ventricular ejection fraction
LVESV	left ventricular end-systolic volume
MI	myocardial infarction
PA	pulmonary artery
PLB	phospholamban

KARGER

E-Mail karger@karger.com
www.karger.com/cto

1422–6405/15/2005–0349$39.50/0

Zhongjun J. Wu, PhD
Department of Cardiovascular and Thoracic Surgery
Cardiovascular Innovation Institute, University of Louisville School of Medicine
Room 410, 302 E. Muhammad Ali Blvd, Louisville, KY 40202 (USA)
E-Mail zhongjun.wu@louisville.edu

Introduction

Acute myocardial infarction (MI) is one of the primary causes of mortality in many developed and developing countries around the world. Cardiac remodeling after MI is a time-dependent process determined by multiple factors, including the status of the nonoccluded coronary arteries, performance of the viable myocardium, location of the infarct [Corr et al., 1975], as well as the size of the infarct itself [Pfeffer et al., 1979]. A large infarct is a high-risk factor for progressive left ventricular (LV) dilatation and adverse events, with approximately 70% of transmural infarcts causing infarct expansion 30 days after MI [Eaton and Bulkley, 1981; Hochman and Bulkley, 1982]. After comparing three groups of patients, Mathey et al. [1974] found larger infarcts were associated with a decrease in the cardiac function and an increase in the mortality rate. The post-MI ventricular function was observed from no discernible impairment to congestive failure based on various MI sizes estimated using planimetry of the endocardial circumference of histological LV slices [Pfeffer et al., 1979]. Mathematical simulation using a finite element method also indicated that cardiac performance degraded with increasing infarct size, and the relationship between infarct stiffness and cardiac function depended on both infarct size and end-diastolic pressure [Carter and Amundsen, 1977; Bogen et al., 1980; Bovendeered et al., 1996]. It was thus suggested the degradation of the ventricular pumping function and hemodynamic performance, as well as the detrimental modifications in LV shape, were proportional to the extent of myocardium affected, which was reported to be independently determined by the ischemic risk region, duration of ischemia, collateral blood flow and myocardial oxygen demand [Christian et al., 1992; Hasche et al., 1995].

The assessment of regional myocardial function is important in detecting incipient ventricular dysfunction, infarct extension and progressive myopathic processes after MI [Gallagher et al., 1987]. There is increasing evidence that the wall stress from myocardial stretch (strain) during cardiac remodeling induces myocyte cell loss, side-to-side slippage and hypertrophy of myocytes, contributing to progressive ventricular dilation and systolic dysfunction [Bing, 1994; Qin et al., 2005]. Radiopaque marker implantation [Rodriguez et al., 2004], tissue Doppler imaging [Yu et al., 2004], magnetic resonance imaging [Carlsson et al., 2008] and digital sonomicrometry [Yeon et al., 2001] have been applied to analyze local strain and strain rate, which define regional structural deformation. Abnormal strain patterns, together with a decrease in the wall thickening and elevated wall stress, were demonstrated in the myocardium adjacent to the acutely ischemic zone [Nicolosi and Spotnitz, 1988; Lessick et al., 1991; Rodriguez et al., 2005; Cheng et al., 2006], which parallels regional myocyte hypertrophy post-MI [Kramer et al., 1998]. However, the influence of infarct size on regional myocardial strain and cardiac hypertrophy, which should facilitate the understanding of cardiac remodeling after MI, still requires elucidation.

The present study was undertaken to identify the effects of infarct size on the cardiac global function, regional myocardial strain, cardiomyocyte size and calcium handling proteins in the infarcted heart in an ovine model. The progressive structural and functional alterations in the different myocardial zones were analyzed during the 12-week study duration. The correlations among ventricular performance, myocardial strain and myocyte size were investigated with infarct size as an independent determinant.

Methods

Thirty-five male Dorset hybrid sheep (weight 55 ± 5 kg) were studied. A left thoracotomy was performed to create an apical infarction with MI sizes of 15, 25 and 35% (32 sheep in three groups). There was a 25% attrition rate due to intraoperative arrhythmia, ventricular fibrillation, hemorrhage, postoperative infection and instrumentation failure. However, the study was completed to assure that each MI group had 8 sheep surviving to the 12-week study duration. Those early terminated animals were excluded from the data analysis. Three animals without MI served as a healthy control group. All the sheep had 16 sonomicrometrical transducers implanted on the LV free wall. The sonomicrometry data were collected twice a week during the course of the 12-week study. At termination, myocardial tissue samples were harvested for analyzing myocardial hypertrophy and calcium handling proteins in the adjacent and remote regions relative to the infarct. Echocardiography was performed before and 30 min after MI, and at termination to quantify the global cardiac function.

Surgical Procedure

Anesthesia was induced with thiopental sodium (10–15 mg/kg i.v.). The sheep were intubated and mechanically ventilated with oxygen (Draeger Anesthesia Monitor; Draeger, Telford, Pa., USA). Anesthesia was maintained with isoflurane (1–3%). Surface ECG, arterial blood pressure, pulse oximetric saturation and esophageal temperature were continuously monitored during the surgical procedure.

MI was created with the ligation of the left anterior descending artery. All coronary artery branches feeding the heart apex were ligated at approximately 2/5, 1/2 and 3/5 of the ventricular length (from apex to base), resulting in 10–15, 20–25 and 30–35% apical MI, respectively. Sixteen transducers (piezoelectrical crystals 2 mm in diameter) for sonomicrometry were sutured onto LV mid-myocardium from apex to base, and from the an-

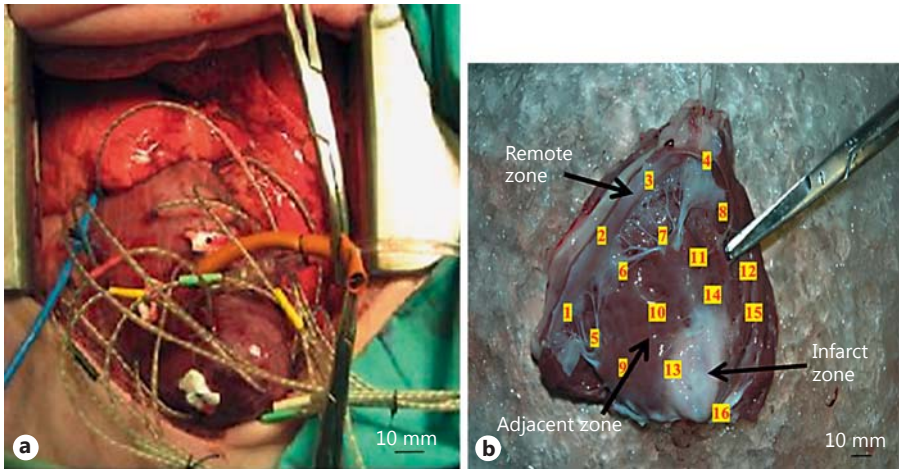

Fig. 1. Sixteen crystals were implanted on the free wall of the LV (**a**) and dissection of LV myocardium at termination (**b**). Number 1–16 delimitated the approximate positions of the 16 sonomicrometric crystals. Crystal 16 was located at the apex and crystal 1 was proximal to the mitral valve plane. The infarct zone was delimited by crystals 13–16. The adjacent zone was within less than 2 cm from the border of the infarct zone and covered by crystals 9–15. The remaining crystals (1–8) enclosed the remote zone. Fibrosis tissue appeared to be white in the infarct zone located at the apical myocardium.

terior to the posterior wall (fig. 1a). An ultrasound flow probe (Transonic Systems Inc., Ithaca, N.Y., USA) was placed around the main pulmonary artery (PA) for cardiac output monitoring. Details on the surgical procedures have been published previously [Yankey et al., 2008]. All the surgical procedures and animal care were carried out according to the protocol approved by the Institutional Animal Care and Use Committee of the University of Maryland School of Medicine and in compliance with the *Guide for the Care and Use of Laboratory Animals* published by the National Institutes of Health (NIH publication No. 85-23, revised 1996).

Echocardiographic Data Collection

A transthoracic two-dimensional echocardiogram was performed using commercially available ultrasound systems (VIVID Q; GE Healthcare, USA). Ventricular images were recorded through both the parasternal short-axis and orthogonal long-axis views. Longitudinal four-chamber scanning was performed through the aortic valve to the apex, whereas short-axis images were attained at the levels of the mitral valve, papillary muscle and apex. All echocardiographic images were acquired over five consecutive heart beats and were digitally stored in DICOM format. Offline image analysis was performed using EchoPAC Dimension software (GE Healthcare).

LV end-diastolic volume (LVEDV), LV end-systolic volume (LVESV) and LV ejection fraction (LVEF) were calculated based on the modified Simpson's biplane principle. The intraoperative infarct size immediately after MI was approximately controlled and examined via the ratio between akinesis/hypokinesis length and endocardial circumference at the mid-papillary level.

Sonomicrometry System

A digital sonomicrometry system (Sonometrics Corp., London, Ont., Canada) was utilized to measure the time-varying segmental distances between one pair from the 16 crystals in the LV during continuous cardiac cycles. The implanted transducers transmitted and received pulsed ultrasonic energy and the ultrasound flight time was recorded by a digital counter. With the knowledge of the ultrasound speed in the tissue, the distances among transducer pairs were measured. Real-time distance traces between pairs from the sixteen transducers were synchronized with PA flow and acquired at a sample rate of 200/s.

An iterative filtering of a multidimensional scaling algorithm was utilized to convert sets of distance measurements into the time-varying 3D coordinates of the transducers from the segmental distances between the transducer pairs. The LV myocardium was anatomically divided into 3 regions: infarct zone (apical myocardium), adjacent zone (<2 cm from the infarct zone) and remote zone (most basal plane). Contractile strain ε_{con} and remodeling strain ε_{rem} (defined in equations 1 and 2) were calculated to characterize contractile function and structural alterations in myocardial regional tissue during progressive remodeling.

$$\varepsilon_{con} = \frac{S_{ED} - S_{ES}}{S_{ED}} \times 100\% \quad (1)$$

$$\varepsilon_{rem} = \frac{S_{ED} - S_{EDpre\text{-}MI}}{S_{EDpre\text{-}MI}} \times 100\% \quad (2)$$

S_{ED} and S_{ES} are the in-plane areas of the myocardial wall at the instants of end diastole (ED) and end systole (ES). $S_{EDpre\text{-}MI}$ is the in-plane area of the myocardial wall at the ED instant before MI.

The in-plane area in a particular area was calculated from the triangle formed by 3 neighboring crystals. Both contractile and remodeling strains are in-plane areal strains, combining both the circumferential and longitudinal deformations. The instants of ED and ES were identified from the simultaneously recorded PA flow trace and the continuous areal waveforms of the myocardial wall. The contractile strain ε_{con} describes the regional myocardial contractive function over the cardiac cycle at a specific time point after MI, while remodeling strain represents the change in the LV in-plane area over time in comparison with the reference configuration before MI. The areal contractile strain is similar to segmental fractional shortening, representing an in-plane areal contraction. The contractile and remodeling strains together with the positions of the implanted transducers can be plotted in a 3D map to represent the regional contractile function and the regional myocardial wall expansion at a time point of interest after MI.

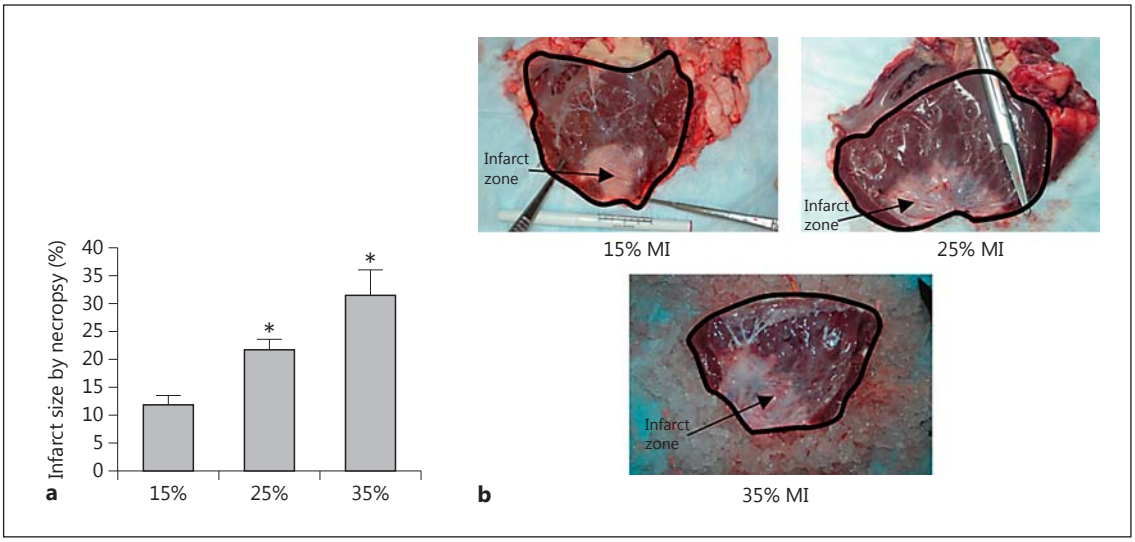

Fig. 2. a Infarct size analysis at the termination expressed as the area ratio between the scar area at the apex and whole LV free wall using ImageJ software. **b** Typical necropsy images of the LV free wall with various infarct sizes. * $p < 0.05$ compared between two groups.

Necropsy, Histology and Protein Analyses

At the time of termination, the heart from each animal was harvested after infusion of cold cardioplegia. The LV myocardium was dissected and photographed. The infarct size was measured as the area ratio between the white scar at the LV apex (indicated by the black arrow as 'infarct zone' in fig. 2b) and the LV free wall (demarcated by a black curve in fig. 2b) using image analysis software (ImageJ; National Institutes of Health, USA). Tissue sections were taken from the remote and adjacent zones of the LV myocardium. A portion of the collected tissues was frozen in liquid nitrogen and stored at –80°C for the analysis of calcium handling proteins. After completion of animal experiments, the frozen tissue samples were processed for probing the expression of the following calcium handling proteins: SERCA2a, NCX-1 and phospholamban (PLB) with Western blotting. Details of protein extraction and Western blotting were described previously [Kilic et al., 2006; Yankey et al., 2008; Yao et al., 2015]. The tissues for histological analysis were washed in PBS and fixed in neutral buffered formalin for 48 h prior to processing [Shan et al., 2008; Pu et al., 2013]. Paraffin-embedded sections were cut at 5 μm and stained with hematoxylin and eosin (HE) and Masson's trichrome. The HE-stained slides were visualized using an Axioskop 50 Zeiss microscope. Images of the tissue slides were digitally recorded. The microscope lighting and focus were optimized to be able to distinguish cell boundaries. The size of individual cardiomyocytes was determined from the recorded images using the ImageJ software. Each cardiomyocyte was manually demarcated and bucket filled in GIMP. The demarcated area of individual cardiomyocytes was automatically calculated using the functions in the ImageJ software [Bogen et al., 1980]. One hundred cardiomyocytes from both the remote and the adjacent section were selected. For collagen content measurement, the recorded images of Masson's trichrome-stained tissue sections were analyzed using the ImageJ software. The fraction of collagen per field (10 fields randomly selected from each section) was determined by dividing the total area of blue-stained collagen by the total area of the tissue viewing field [Berry et al., 2006].

Statistics

All data are expressed as the mean ± SEM. Comparisons of the global cardiac function parameters, myocardial strains and cardiomyocyte sizes were performed by ANOVA. The comparisons were performed to test the significance of differences between different locations at the same time points or between different groups from the same topographic location at different times. Strain data were correlated with echocardiographic measurements and cardiomyocyte sizes. Post hoc analysis was performed using the Newman-Keuls method; significance was set at $p < 0.05$.

Results

Infarct Size

The infarct sizes were determined by the planimetry at necropsy as 12 ± 2, 22 ± 2 and 30 ± 4% for the three MI groups (fig. 2). The difference in the infarct size between the groups was significant ($p < 0.05$). These MI groups were designated later as 15, 25 and 35% groups, respectively.

Echocardiographic Measurements

Echocardiographic images from the sham, and 15, 25 and 35% MI groups were analyzed for LV volumes and cardiac function. The data derived from the echocardio-

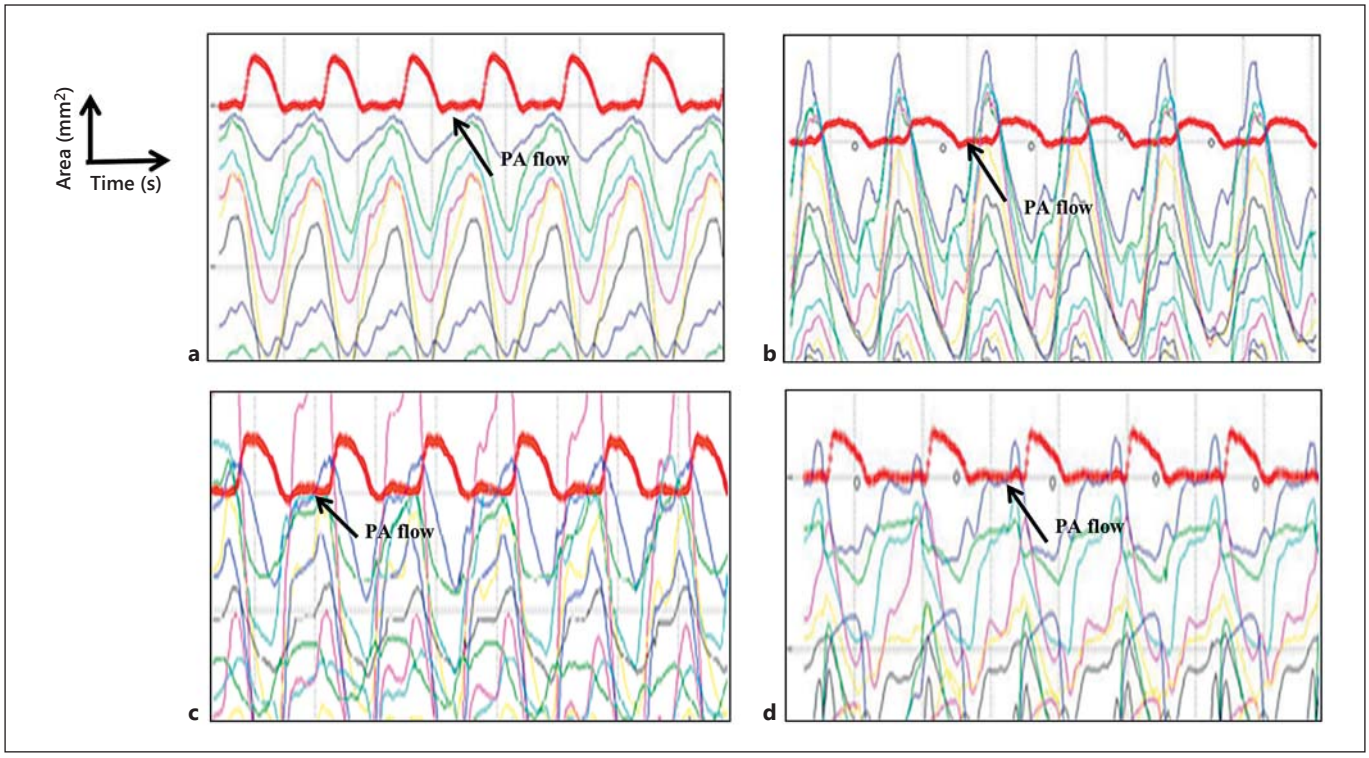

Fig. 3. Representative areal waveforms before MI (**a**), and at 15% MI (**b**); 25% MI (**c**) and 35% MI at the 12th week (**d**), respectively. Note that every myocardial sectional areal waveform was displaced 10 mm^2 upward from the previous one for better visualization.

Table 1. Echocardiographic quantification of LV volume and function and hemodynamic measurements in the study groups

	Sham		15% MI		25% MI		35% MI	
	pre-MI	termination	pre-MI	termination	pre-MI	termination	pre-MI	termination
Normalized LVEDV, ml/kg	1.4±0.1	1.5±0.2	1.2±0.2	1.4±0.2*	1.3±0.2	1.7±0.3*, &	1.5±0.2	2.0±0.4*, &, #
Normalized LVESV, ml/kg	0.6±0.01	0.8±0.1	0.5±0.1	1.0±0.1*, &	0.6±0.1	1.0±0.2*, &	0.6±0.1	1.3±0.3*, &, #
Normalized SV, ml/kg	0.8±0.1	0.8±0.1	0.7±0.1	0.8±0.1	0.7±0.1	0.7±0.1	0.6±0.1	0.7±0.1
Cardiac output, ml/(min × kg)	69±7	70±7	70±14	72±13	73±7	71±18	65±11	67±9
LVEF, %	56±2	53±2	57±2	43±3*, &	55±2	42±6*, &	54±3	34±4*, &, #
Mean arterial pressure, mm Hg	74±11	74±7	77±16	78±10	68±9	68±16	67±6	78±10*
Systolic pressure, mm Hg	79±3	78±20	84±9	84±13	85±12	85±20	83±9	92±12*, &, #
Diastolic pressure, mm Hg	56±9	58±11	59±11	58±4	58±9	57±14	55±1	67±12*, &, #
Heart rate, beats/min	104±1	104±6	112±8	117±14&	99±15	103±10	102±10	101±14

SV = Stroke volume. * $p < 0.05$ for the same group at the pre-MI vs. at termination, & $p < 0.05$ for the MI group vs. the sham group at termination, # $p < 0.05$ between the MI groups at termination.

graphic images are presented in table 1. LVEDV, LVESV, stroke volume and cardiac output were normalized by body weight. The sham group had negligible differences in all the parameters between the times before MI and at termination. For the three MI groups, the differences in LVEDV, LVESV and LVEF were significant between the times before MI and at termination. In comparison with the 15% group, the 35% MI group exhibited larger LVEDV, LVESV and remarkably reduced LVEF ($p < 0.05$). Additionally, the systolic and diastolic pressures in the 35% MI

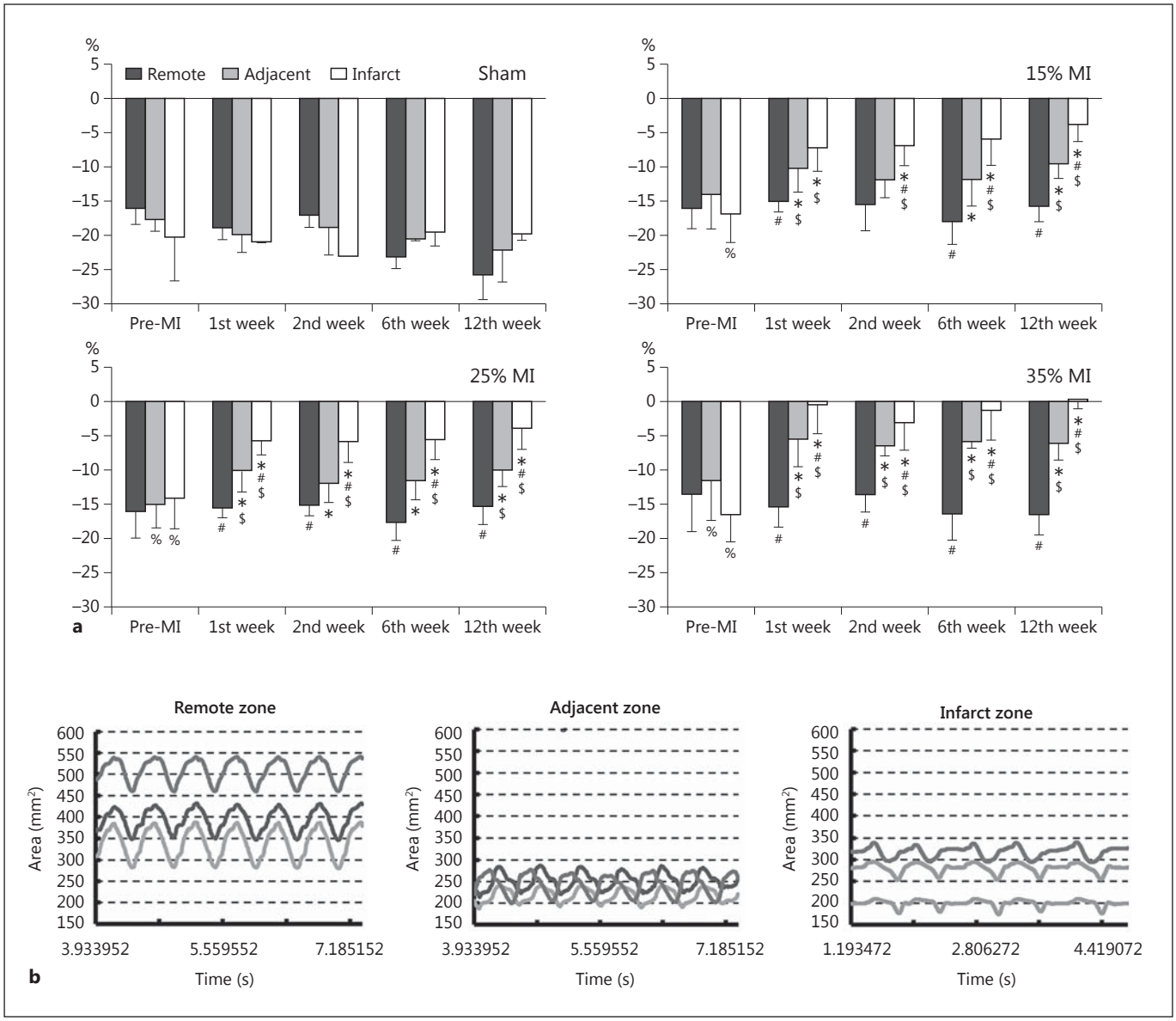

Fig. 4. a Contractile strain of the sham, and 15, 25 and 35% MI groups. **b** Typical myocardial areal waveforms from the remote, adjacent and infarct zones at the termination in the 25% MI group. * $p < 0.05$ vs. remote zone, # $p < 0.05$ vs. adjacent zone, $ $p < 0.05$ vs. before MI, % $p < 0.05$ vs. 6th week.

group are statistically higher than those in the 15% MI group. However, for all the MI groups, the measurements of normalized stroke volume, cardiac output and mean arterial pressure at the termination did not show significant differences from those obtained before MI.

Myocardial Asynchronous Motion

Asynchronous motion across the LV free wall was noted after MI. Representative areal waveforms of the LV wall over 5–7 continuous cardiac cycles are shown in figure 3. These waveforms represent in-plane areas of individual triangles that were constructed from three adjacent sonomicrometry transducers and covered the LV free wall. The periodic maximum and minimum values on every waveform represented the regional ED and ES instants of cardiac cycles. Before MI, the myocardium showed good repeatability, similarity and synchronicity, while asynchronous motion was observed among myo-

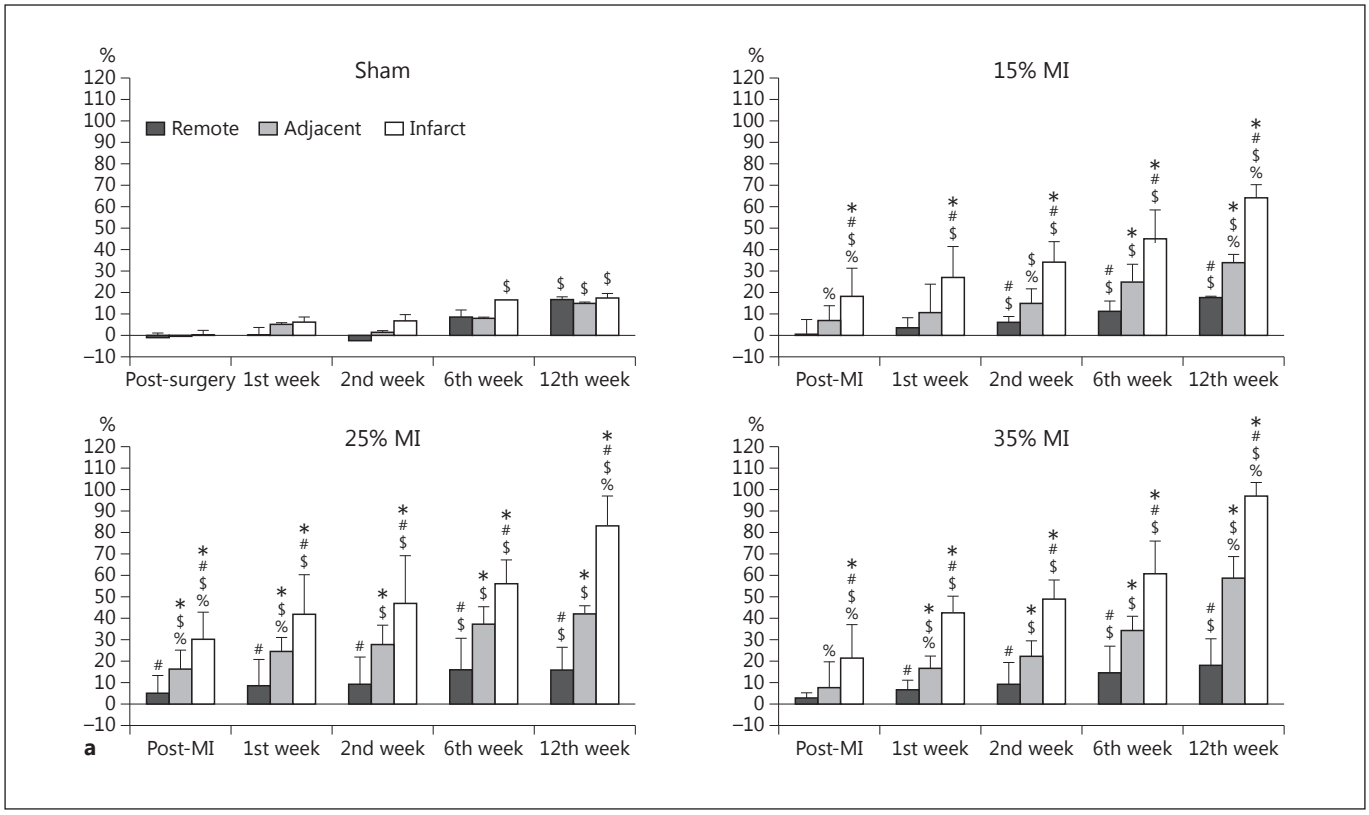

Fig. 5. a Temporal changes in the remodeling strains of the sham group and the three MI groups at the five time points after MI (1st, 2nd, 6th and 12th week). * $p < 0.05$ vs. remote zone, # $p < 0.05$ vs. adjacent zone, $ $p < 0.05$ vs. pre-MI, % $p < 0.05$ vs. 6th week.

cardial sections at the 12th week after MI, with varied ED and ES instants at different myocardial regions. The asynchrony tended to worsen with the increase in infarct size. Thus, the ED and ES instants were individually chosen for individual regions of the LV myocardium in the strain calculation after MI.

Sonomicrometry Strain Analysis

Contractile Strain

Figure 4a shows the trends of the contractile strain in the three zones of the LV over the 12-week study period for the sham group and the three MI groups. The sham group exhibited similar strain magnitudes among the remote, adjacent and infarct zones, with a value around –15 to –25% at the termination. The 15, 25 and 35% MI groups showed a continuous decrease in the contractile strain in the adjacent and infarct zones after MI. The contractile strain in the remote zone of the three MI groups remained almost unchanged over the 12-week study period. However, the infarct zone lost the viable contractile function immediately after MI. The adjacent zone also suffered after MI. However, the adjacent zone of the 35% MI group had a much higher reduction in the contractile function compared to those of the 15 and 25% MI groups. Although there were not contracting myocytes in the infarct zone, the motion of the infarct zone could have affected neighboring tissue since the scar was enclosed in the viable myocardial tissue, i.e. adjacent myocardium, septal wall and right ventricular free wall. When these tissues contract, they might contract the scar too. Therefore, a small contractile strain was observed in the infarct zone when the infarct size was small.

Figure 4b shows typical myocardial areal waveforms at the 12th week in the remote, adjacent and infarct zones of the 25% MI group. The magnitudes of the contractility were 86, 63 and 35 mm^2 in the remote, adjacent and infarct zones, respectively. The corresponding velocities of the contractility were 815, 566 and 272 mm^2/s. The magnitude and velocity of the contractility were found to be continuously decreasing in the adjacent and infarct re-

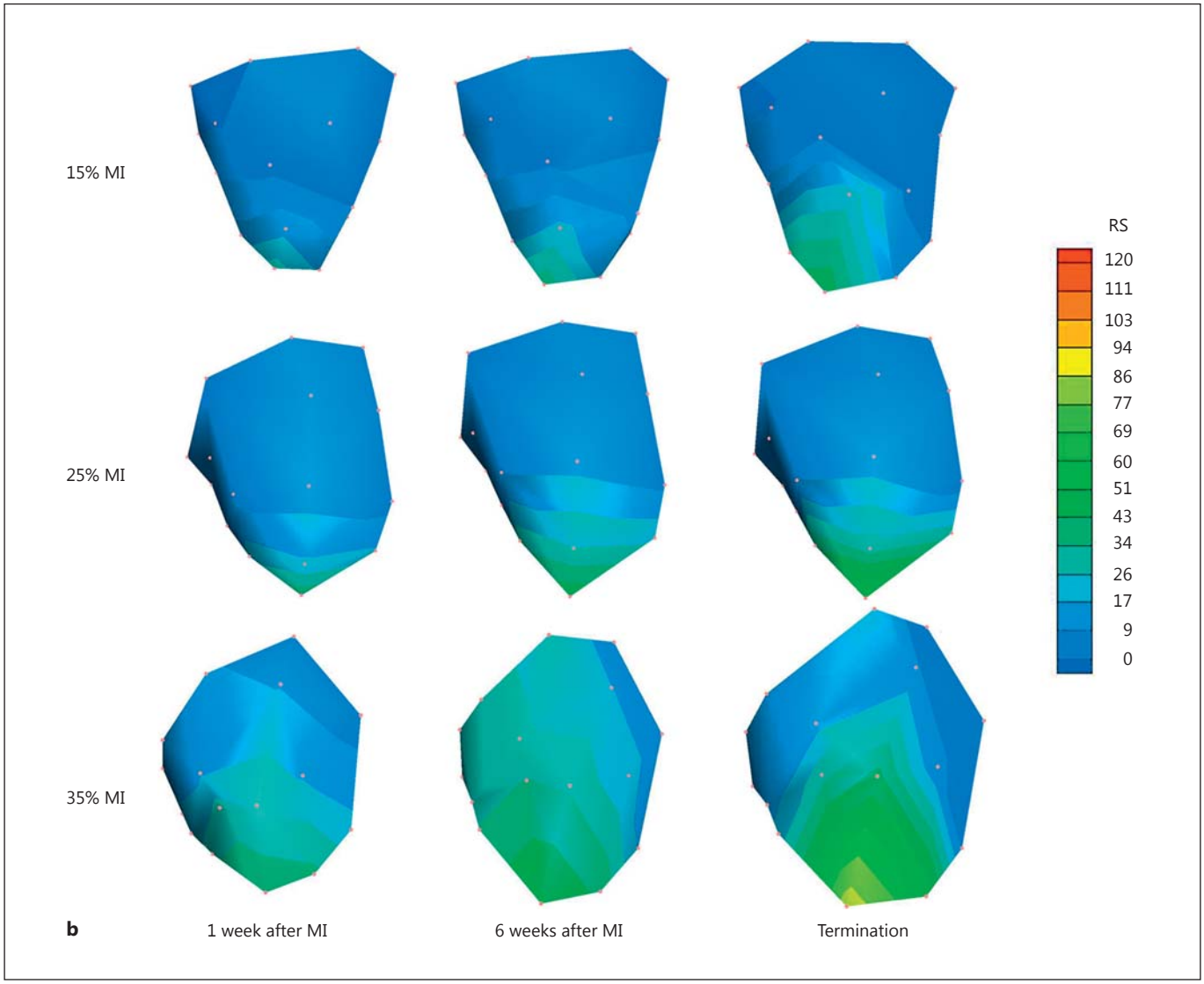

Fig. 5. b Typical 3D contours of the remodeling strain at three time points after MI (1st week, 6th week and termination). The color map was created using the interpolation scheme in Tecplot software. The solid dots on the LV free wall represent 16 crystal transducers. The apex is located at the bottom of the LV geometry. The progressive increase in the remodeling strain was found in the adjacent and infarct zones.

gions compared to the remote myocardium. The remote zone also demonstrated synchronous motion among various myocardial sections as indicated by the well-aligned peaks and valleys in the traces. However, the misaligned peaks and valleys, which indicated asynchronous contraction, were observed in the adjacent and infarct zones.

Remodeling Strain

Figure 5a shows the trends of the remodeling strain in the remote, adjacent and infarct zones over the 12-week period for the sham and the three MI groups. The sham group had a small regional variation in the remodeling strain, with a magnitude around 15–20% 12 weeks after MI. In comparison, the 15, 25 and 35% MI groups had the remodeling strain around 34, 42 and 59% in the adjacent zone, and around 64, 83 and 97% in the infarct zone 12 weeks after MI, respectively. In the remote zone, the remodeling strain was similar to that of the remote zone of the sham group. In comparison with the 15% MI group, the 35% MI group showed significantly different

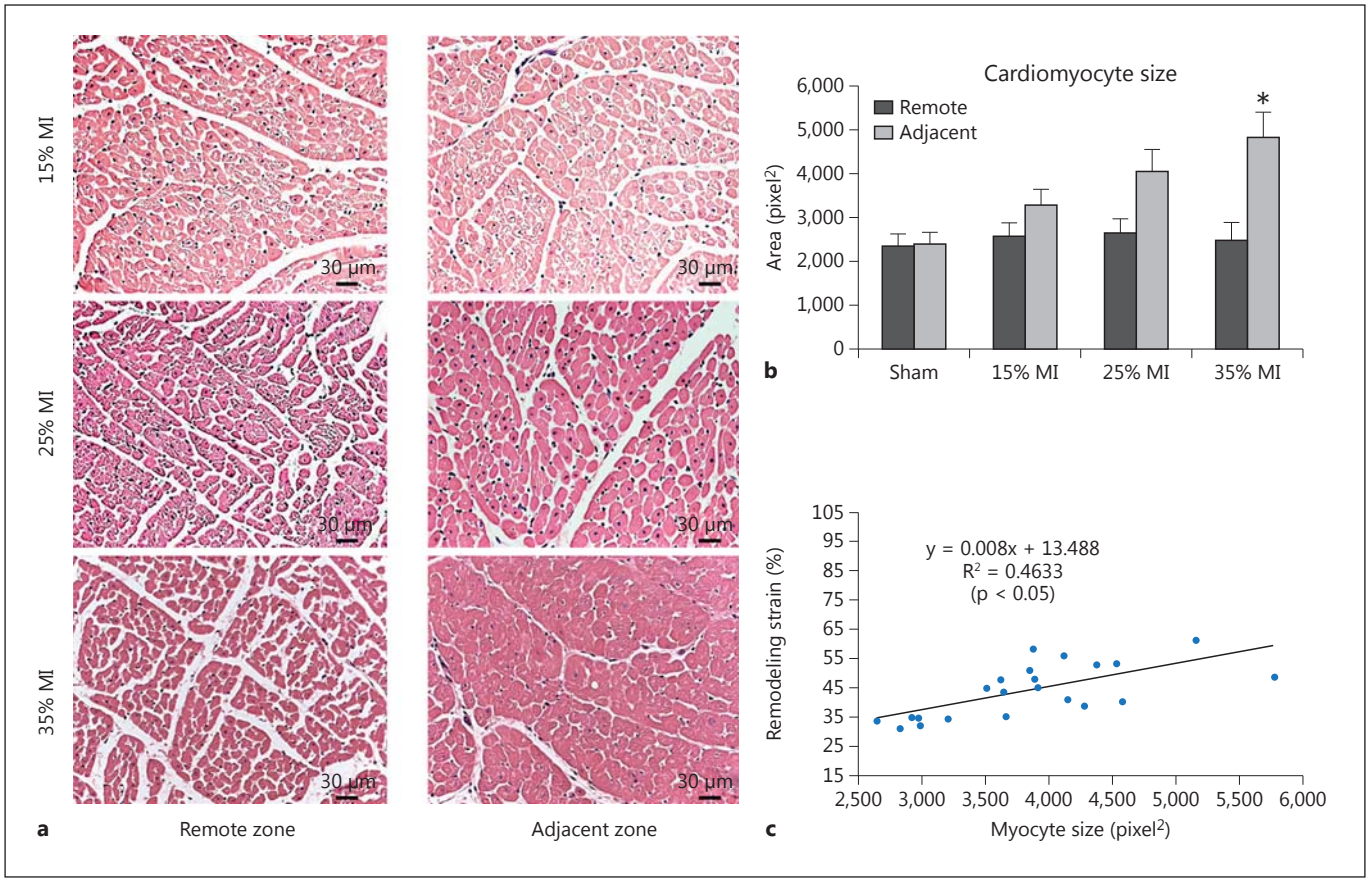

Fig. 6. a Typical images of HE-stained myocardial tissue from the remote and adjacent zones of the three MI groups. **b** Comparison of the cardiomyocyte sizes in the remote and adjacent zones in the sham group and the three MI groups. **c** Correlation between cardiomyocyte size and remodeling strain in the adjacent zone of the three MI groups. * $p < 0.05$ 15% vs. 35% MI group.

remodeling strain in both the adjacent and infarct zones ($p < 0.05$) for most time points during the 12-week period.

Figure 5b shows typical 3D remodeling strain maps of the three MI groups at three time points after MI. The largest remodeling strain located at the apex and progressively propagated from the apex to the adjacent zone. The myocardial remodeling in the remote zone over time was minimal. The progressive remodeling trend at the apex of the LV free wall can be seen for the three MI groups, indicating local myocardial expansion over time.

Cardiomyocyte Size

The myocardium in the adjacent zone of all the three MI groups had a larger cardiomyocyte size compared to that in the remote zone. The enlarged cardiomyocytes in the adjacent zone of the three MI groups compared with the remote zone can be seen in typical images of the HE-stained tissue sections (fig. 6a). A statistical difference was also found in the adjacent zone between the 15 and 35% MI groups (fig. 6b).

Correlations between Regional Strain and Cardiomyocyte Size

The cardiomyocyte size in the adjacent zone was found to correlate with the remodeling strain ($p < 0.05$; fig. 6c). This may suggest that the overall geometry and remodeling was associated with the underlying cellular structure change.

Masson's Trichrome Staining

Typical images of trichrome-stained tissue sections in the remote and adjacent zones for the 15, 25 and 35% MI groups are shown in figure 7. The collagen amount in the

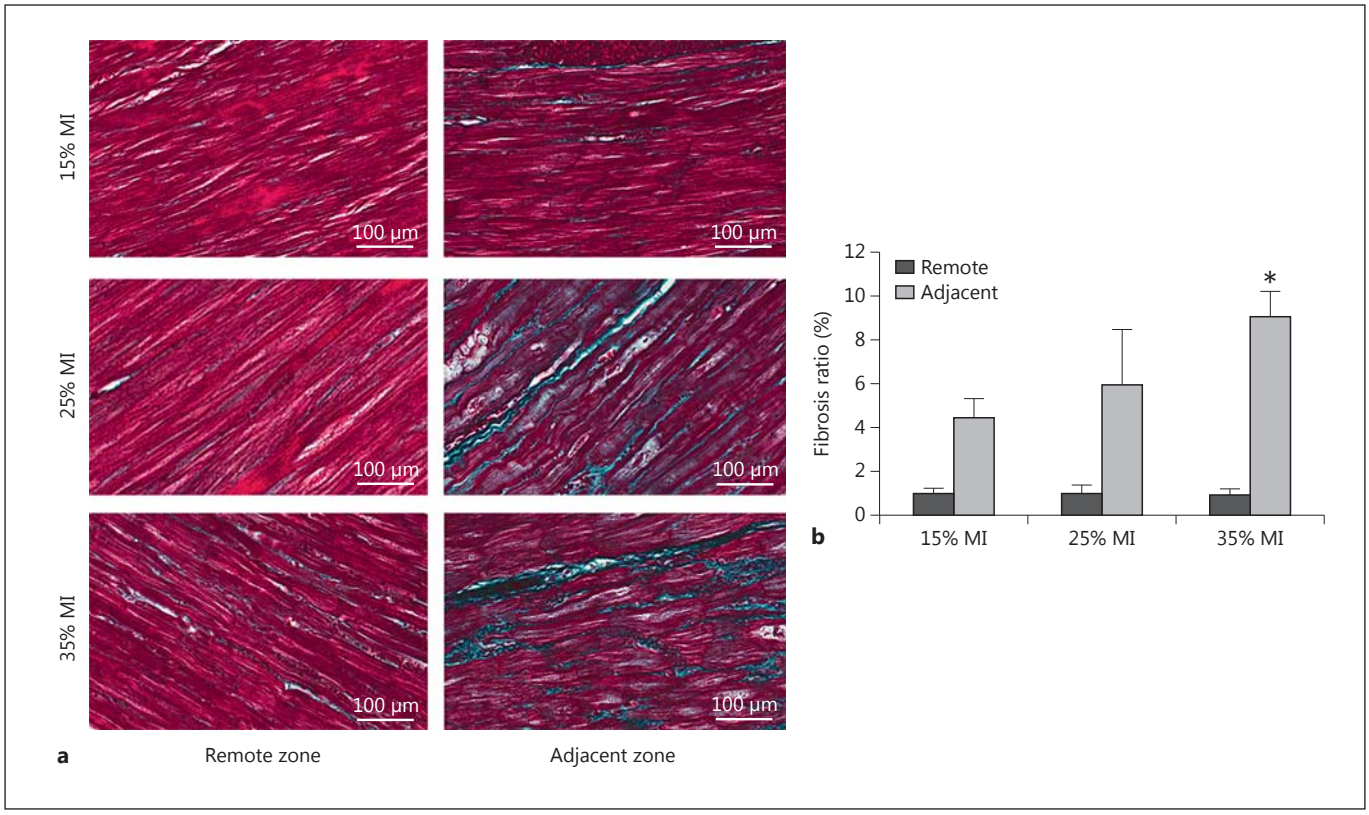

Fig. 7. a Typical images of the Masson's trichrome-stained myocardial tissues in the remote and adjacent zones from the three MI groups. **b** Comparison of the fibrosis ratio in the remote and adjacent zones among the sham group, and 15, 25 and 35% MI groups. * $p < 0.05$ 15% vs. 35% MI group.

remote zone among the three MI groups was less than 1%. Differences in the collagen amount in the remote zone among the three MI groups were negligible. However, the collagen content (fibrosis) increased significantly in the adjacent zone among the three MI groups. The ratio of fibrotic area was higher in the 35% MI group than in the 25 and 15% MI groups.

Calcium Handling Proteins

Figure 8 shows the abundance of the major calcium-regulatory proteins, SERCA2a, PLB and NCX-1 in the adjacent and remote zones of the remodeling myocardium of the sham group and the three MI groups. SERCA2a and PLB were all significantly down-regulated in the adjacent zone of all the three MI groups compared to the sham group ($p < 0.05$), while NCX-1 was significantly up-regulated. Among the three MI groups, the differences in the abundance of the three major calcium handling proteins were found to be significant between the 15 and 35% MI groups.

Discussion

In this work, we used echocardiography, sonomicrometry, histology and molecular biology approaches to characterize the influence of infarct size on global cardiac function, LV geometry, regional contractile function, regional geometry, regional cardiomyocyte size and contraction-related calcium handling proteins of the infarcted hearts during a 12-week remodeling course. The extent of LV dilation and cardiac dysfunction after MI was related to the magnitude of the initial damage to the myocardium, which is in agreements with previous studies [Jugdutt et al., 1996; Patten et al., 1998]. The magnitudes of regional myocardial contractile strain in the infarct and adjacent zones were found to be directly related to the loss and down-regulation of the major calcium handling proteins in the myocardium.

Significantly different remodeling strain and contractile strain in both the adjacent and infarct zones were observed between the 15 and 35% MI groups. Hypertro-

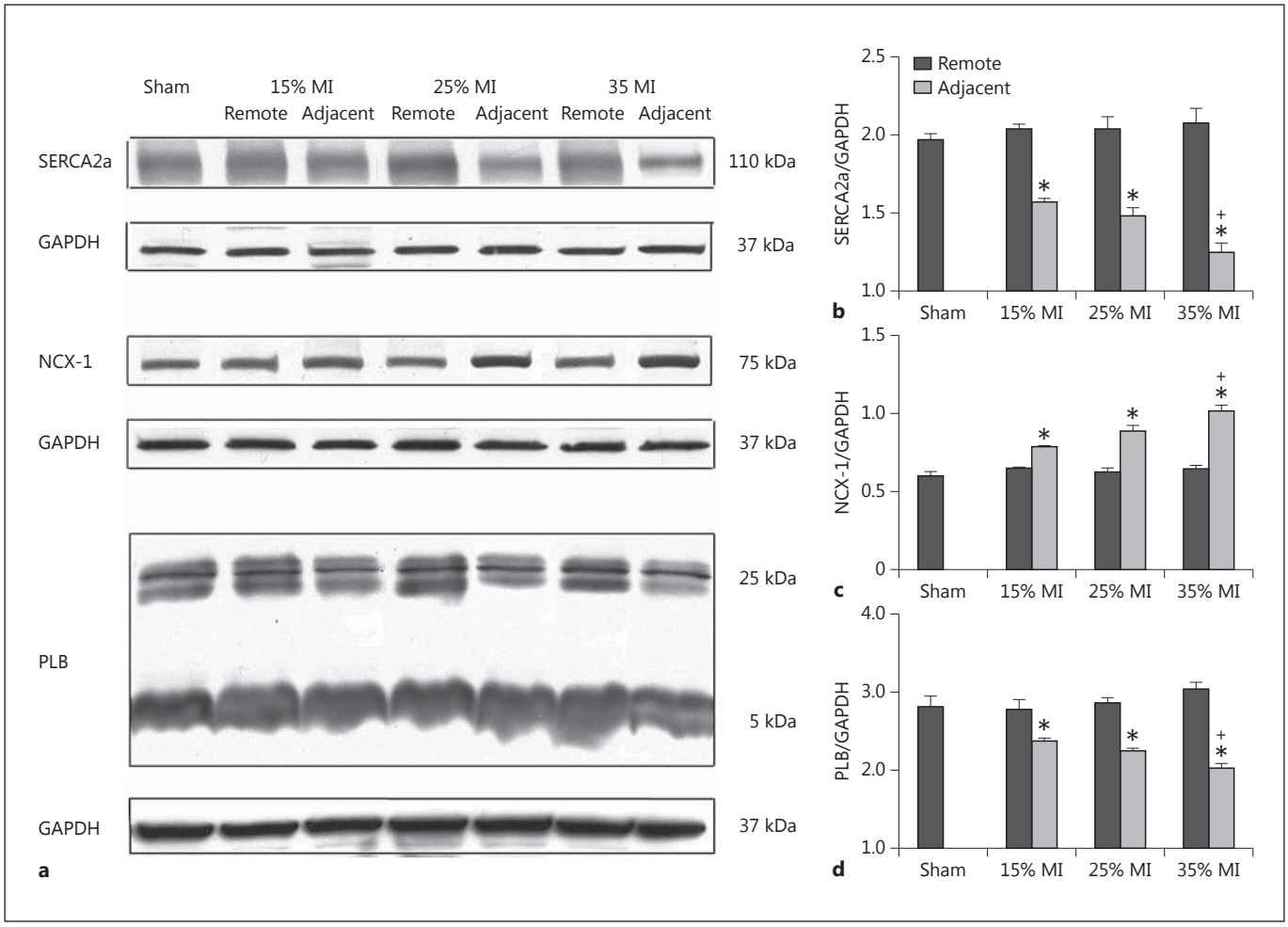

Fig. 8. a Typical pictures of Western blots for calcium handling protein expression. Comparisons of SERCA2a (**b**), NCX-1 (**c**) and the PLB pentamer (**d**) between the adjacent and the remote zone among the sham group and the three MI groups. * $p < 0.05$ vs. the remote zone or the sham group, $^{+}$ $p < 0.05$ vs. the adjacent zone in the 15% MI group only.

phic cardiomyocytes were found in the zone adjacent to the infarcted myocardium. In parallel, the enlarged myocardium (increased remodeling strain) was observed in the adjacent zone. A significant correlation was found between the cardiomyocyte size and the remodeling strain in the adjacent zone. Meanwhile, the 35% MI group was observed to have a higher fibrosis ratio in the adjacent zone than the 15 and 25% MI groups. We thus believe that the infarct size is an important factor for cardiac remodeling after MI and should be considered a risk factor for ventricular dilation, dysfunction, myocyte hypertrophy and fibrosis development, as well as other adverse effects.

Myocardial Asynchrony

Digital sonomicrometry, with improved temporal (>125 Hz) and spatial resolution (0.024 mm), was applied in this study to measure the strain variations among regional myocardium and to enable the measurements obtained under conscious conditions. With well-defined ED and ES instants individually selected from various myocardial regions, the effect of the myocardial asynchrony on the regional strain measurement was minimized, specifically for the large infarct size at a late time after MI. Asynchronous myocardial motion, which commonly occurs in ischemic heart disease, was however seldom taken into account in these types of studies, possibly causing some discrepancies in the evaluation of the local

myocardial behavior [Sugihara et al., 2005]. The current work demonstrated cardiac dyssynchrony among various regions of the myocardium demarcated by 16 transducers on the LV free wall. It was found that with the increase in MI size and progression of the remodeling process, myocardial asynchrony tended to exacerbate, possibly resulting from the dramatically varied contractility among the remote, adjacent and infarct zones. This was manifested by the diversity of the regional contractile strain, as well as the various magnitudes and velocities of myocardial deformation shown on the regional areal waveforms.

Myocardial Regional Remodeling Strain

Local myocardial deformation was measured by a sonomicrometry system together with a planar areal strain analysis approach. The sonomicrometry technique was invasive to the myocardial tissue, but its detrimental effect on the alterations in myocardial function can be neglected since the strains in the remote zone did not show a significant change over the 12-week study period after placing the crystals on the myocardium. Additionally, the calculation of 2D areal strain deformation was adopted from previously published studies and the local planar strains were found correlating with the alterations in the protein pathway [Kilic et al., 2006] and myocyte loss [Yankey et al., 2008] in the corresponding zones. The remodeling strain distributions in the various regions of the LV represent the characteristic functional and structural properties of the myocardium, which is composed of myocytes, fibroblasts, extracellular matrix and coronary vasculature. Kramer et al. [1998] found that LV dilation and hypertrophy were associated with segmental differences between different myocardial tissues, while Fernandes et al. [2007] reported LVEF was directly related to the magnitude of circumferential contractile strain, and LVESV showed an inverse relationship with contractile strain and rate. Ratcliffe [2002] also pointed out that alterations in remodeling strain could cause myocyte extension and initiate myocyte apoptosis, which was prone to reduce the contractility of the myocardium adjacent to the infarct. We speculate that the myocardial remodeling strain is an initial impetus not only behind the organ impairment of LV geometry and function, but also behind the cardiomyocyte hypertrophy and possible cell death during progression of cardiac remodeling, with infarct size as an important determinant of the ventricular performance at organ, tissue and cell levels. As the LV cavity progressively becomes enlarged, the efficiency of LV pumping was reduced. According to the Laplace principle, the myocardial tissue would experience higher mechanical stress with a larger LV chamber under the same arterial pressure afterload. Thus, myocardial strain/stress reduction through LV assist devices, passive epicardial constraint devices and surgical LV restoration procedures would result in reversal of cardiac remodeling and restoration of ventricular function [Athanasuleas et al., 2001; Razeghi et al., 2002; Sabbah et al., 2003; Wei et al., 2013].

It is worthwhile to mention that in all the three MI groups the maximum strain gradients were observed within 2 weeks after MI. In comparison with healthy subjects, Erlebacher et al. [1984] found that both anterior and posterior segment lengths were significantly different within 72 h of infarction, while negligible difference was shown between early and late in-hospital studies (9–21 days). In a 1-year follow-up study after MI with measurements performed at baseline, and after 3, 6 and 12 months, statistically different longitudinal peak systolic (contractile) strain was presented between baseline and the 3rd month as well as the 3rd and the 12th month, while the measurement at the 6th month did not differ from those at 3 and 12 months [Antoni et al., 2010]. Our results are in qualitative agreement with the above-mentioned works considering the differences in the species genre, methodology and time schedule. We thus suggest an early prevention of ventricular remodeling, within 2 weeks after infarction, is an optimized time window for any preemptive medical or surgical strategies, which have been confirmed by numerous studies. When either mechanical constraint of cardiac support device [Cheng et al., 2006], therapeutic agents as captopril [Pfeffer et al., 1985], or reperfusion and thrombolysis [Simoons et al., 1986; Takiuchi et al., 1998] was administrated immediately after MI, the LV demonstrated remarkably reduced remodeling strain/dilation and substantially improved cardiac functions and survival rate. Harada et al. [2005] indicated that the delayed treatment of granulocyte colony-stimulated factor on cardiomyocytes after MI would cause less beneficial effects of granulocyte colony-stimulating factor on ventricular function.

Limitations

The areal strain approach was one of the study limitations when applied to describe the 3D ventricular myocardial deformation. The asynchronous myocardial motion needs to be further quantified to better understand the cardiac remodeling after MI. The small number of animals in the sham group might cause relatively larger variations in the regional strain calculations in the sham group.

Conclusion

The global cardiac function, LV geometry, regional contractile function and geometrical remodeling strain, regional hypertrophy and molecular functional proteins of infarcted hearts with the three MI sizes were characterized combining bioengineering and biological approaches. The reduced regional myocardial contractile function in the zone adjacent to the infarct was found to be related to the decrease in major calcium handling proteins. In the same notion, the alteration in the geometry in the adjacent zone (enlargement) was observed to be corresponding to the enlarged cardiomyocytes in the same zone. Asynchronous motions among various myocardial regions after MI were observed. The infarct size was found to be very important for cardiac remodeling after MI, which also affected the infarcted hearts at multiple levels from the whole organ to the cellular composition, and should be considered as a risk factor for ventricular dilation, dysfunction and myocyte hypertrophy, as well as other adverse effects.

Acknowledgment

This work was funded by the National Institutes of Health (grant No. R01HL081106).

References

Antoni, M.L., S.A. Mollema, et al. (2010) Time course of global left ventricular strain after acute myocardial infarction. Eur Heart J *31:* 2006–2013.

Athanasuleas, C.L., A.W. Stanley Jr, et al. (2001) Surgical anterior ventricular endocardial restoration (SAVER) in the dilated remodeled ventricle after anterior myocardial infarction. J Am Coll Cardiol *37:* 1199–1209.

Berry, M.F., A.J. Engler, et al. (2006) Mesenchymal stem cell injection after myocardial infarction improves myocardial compliance. Am J Physiol Heart Circ Physiol *290:* H2196–H2203.

Bing, O.H. (1994) Hypothesis: apoptosis may be a mechanism for the transition to heart failure with chronic pressure overload. J Mol Cell Cardiol *26:* 943–948.

Bogen, D.K., S.A. Rabinowitz, et al. (1980) An analysis of the mechanical disadvantage of myocardial infarction in the canine left ventricle. Circ Res *47:* 728–741.

Bovendeered, P.H.M., T. Arts, et al. (1996) Regional wall mechanics in the ischemic left ventricle: numerical modeling and dog experiments. Am J Physiol *270:* H398–H410.

Carlsson, M., N.F. Osman, et al. (2008) Quantitative MR measurements of regional and global left ventricular function and strain after intramyocardial transfer of VM202 into infarcted swine myocardium. Am J Physiol Heart Circ Phyiol *295:* H522–H532.

Carter, C.L., L.R. Amundsen (1977) Infarct size and exercise capacity after myocardial infarction. J Appl Physiol *42:* 782–785.

Cheng, A., F. Langer, et al. (2006) Transmural left ventricular shear strain alterations adjacent to and remote from infarcted myocardium. J Heart Valve Dis *15:* 209–218.

Christian, T.F., R.S. Schwartz, et al. (1992) Determinants of infarct size in reperfusion therapy for acute myocardial infarction. Circulation *86:* 81–90.

Corr, P.B., D.L. Pearle, et al. (1975) Site of myocardial infarction. A determinant of the cardiovascular changes induced in the cat by coronary occlusion. Circ Res *39:* 840–847.

Eaton, L.W., G.H. Bulkley (1981) Expansion of acute myocardial infarction: its relationship to infarct morphology in a canine model. Circ Res *49:* 80–88.

Erlebacher, J.A., J.L. Weiss, et al. (1984) Early dilation of the infarcted segment in acute transmural myocardial infarction: role of infarct expansion in acute left ventricular enlargement. J Am Coll Cardiol *4:* 201–208.

Fernandes, V.R., T. Edvardsen, et al. (2007) The influence of left ventricular size and global function on regional myocardial contraction and relaxation in an adult population free of cardiovascular disease: a tagged CMR study of the MESA cohort. J Cardiovasc Magn Reson *9:* 921–930.

Gallagher, K.P., R.A. Gerren, X.H. Ning XH, et al. (1987) The functional border zone in conscious dogs. Circulation *76:* 929–942.

Harada, M., Y.J. Qin, H. Takano, et al. (2005) G-CSF prevents cardiac remodeling after myocardial infarction by activating the Jak-Stat pathway in cardiomyocytes. Nat Med *11:* 305–311.

Hasche, E.T., D. Fernandes, et al. (1995) Relationship between ischemia time, infarct size, and left ventricular function in humans. Circulation *92:* 710–719.

Hochman, J.S., B.H. Bulkley (1982) Expansion of acute myocardial infarction: an experimental study. Circulation *65:* 1446–1450.

Jugdutt, B.I., M.J. Joljart, et al. (1996) Rate of collagen deposition during healing and ventricular remodeling after myocardial infarction in rat and dog models. Circulation *94:* 94–101.

Kilic, A., T. Li, et al. (2006) Strain-related regional alterations of calcium-handling proteins in myocardial remodeling. J Thorac Cardiovasc Surg *132:* 900–908.

Kramer, C.M., W.J. Rogers, et al. (1998) Regional myocyte hypertrophy parallels regional myocardial dysfunction during post-infarct remodeling. J Mol Cell Cardiol *30:* 1773–1778.

Lessick, J., S. Sideman, et al. (1991) Regional three-dimensional geometry and function of left ventricles with fibrous aneurysms: a cine-computed tomography study. Circulation *84:* 1072–1086.

Mathey, D., W. Bleifeld, et al. (1974) Attempt to quantitate relation between cardiac function and infarct size in acute myocardial infarction. Br Heart J *36:* 271–279.

Nicolosi, A.C., H.M. Spotnitz (1988) Quantitative analysis of regional systolic function with left ventricular aneurysm. Circulation *78:* 856–862.

Patten, R.D., M.J. Aronoovitz, et al. (1998) Ventricular remodeling in a mouse model of myocardial infarction. Am J Physiol Heart Circ Physiol *274:* H1812–H1820.

Pfeffer, M.A., J.M. Preffer, et al. (1979) Myocardial infarct size and ventricular functions in rats. Circ Res *44:* 503–512.

Pfeffer, M.A., J.M. Preffer, et al. (1985) Survival after an experimental myocardial infarction: beneficial effects of long-term therapy with captopril. Circulation *72:* 406–412.

Pu, J., A. Yuan, et al. (2013) Cardiomyocyte-expressed farnesoid-X-receptor is a novel apoptosis mediator and contributes to myocardial ischaemia/reperfusion injury. Eur Heart J *34:* 1834–1845.

Qin, F., M.C. Liang, et al. (2005) Progressive left ventricular remodeling, myocyte apoptosis, and protein signaling cascades after myocardial infarction in rabbits. Biochim Biophys Acta *1740:* 499–513.

Ratcliffe, M.B. (2002) Non-ischemic infarct extension: a new type of infarct enlargement and a potential therapeutic target. J Am Coll Cardiol *40:* 1168–1171.

Razeghi, P., T.J. Myers, et al. (2002) Reverse remodeling of the failing human heart with mechanical unloading. Cardiology *98:* 167–174.
Rodriguez, F., F. Langer, et al. (2005) Alterations in transmural strains adjacent to ischemic myocardium during the acute midcircumflex occlusion. J Thorac Cardiovasc Surg *129:* 791–803.
Sabbah, H.N., V.G. Sharov, et al. (2003) Reversal of chronic molecular and cellular abnormalities due to heart failure by passive mechanical ventricular containment. Circ Res *93:* 1095–1101.
Shan, P., J. Pu, et al. (2008) RXR agonists inhibit oxidative stress-induced apoptosis in H9c2 rat ventricular cells. Biochem Biophys Res Commun *375:* 628–633.
Simoons, M.L., P.W. Serruys, et al. (1986) Early thrombolysis in acute myocardial infarction: limitation of infarct size and improved survival. J Am Coll Cardiol *7:* 717–728.
Sugihara, H., Y. Yonekura, et al. (2005) Relationship between asynchronous myocardial contraction and left ventricular systolic and diastolic function – assessment using the ECG-gated polar map with ^{99m}Tc-methoxy-isobutyl isonitrile. Circ J *69:* 183–187.
Takiuchi, S., H. Ito, et al. (1998) Ultrasonic tissue characterization predicts myocardial viability in early stage of reperfused acute myocardial infarction. Circulation *97:* 356–362.
Wei, X., T. Li, et al. (2013) Short-term mechanical unloading with left ventricular assist devices after acute myocardial infarction conserves calcium cycling and improves heart function. JACC Cardiovasc Interv *6:* 406–415.
Yankey, G.K., T. Li, et al. (2008) Regional remodeling strain and its association with myocardial apoptosis after myocardial infarction in an ovine model. J Thorac Cardiovasc Surg *135:* 991–998.
Yao, T., X. Ying, et al. (2015) Vitamin D receptor activation protects against myocardial reperfusion injury through inhibition of apoptosis and modulation of autophagy. Antioxid Redox Signal *22:* 633–650.
Yeon, S.B., N. Reichek, et al. (2001) Validation of in vivo myocardial strain measurement by magnetic resonance tagging with sonomicrometry. J Am Coll Cardiol *38:* 555–561.
Yu, C.M., J.W. Fung, et al. (2004) Tissue Doppler imaging is superior to strain rate imaging and postsystolic shortening on the prediction of reverse remodeling in both ischemic and non-ischemic heart failure after cardiac resynchronization therapy. Circulation *110:* 66–73.